Макрогетероциклы
http://mhc-isuct.ru

DOI: 10.6060/mhc267000L

Porphyrin-Triazine Hybrid and Its Zinc Complex: Spectroscopy, Electrochemistry and *in vitro* Cytotoxic Activities against Head and Neck Squamous Cell Carcinoma

Zhouqun Ji,[a] Yingtan Zhai,[b] Tingting Gu,[b] and Xu Liang[b@]

[a]*Affiliated Hospital of Jiangsu University, Zhenjiang 212000, P. R. China*
[b]*School of Chemistry and Chemical Engineering, Jiangsu University, Zhenjiang 212013, P. R. China*
[@]*Corresponding author E-mail: liangxu@ujs.edu.cn*

*Herein, a porphyrin-triazine hybrid **2** and its zinc complex **2-Zn** were synthesized and characterized, and the electronic structures were investigated by spectroscopic and electrochemical characterizations. Weak interactions between porphyrin cores and meso-substituted triazine units were confirmed and the influence of solvents on the spectroscopic properties were also discussed. Importantly, these two porphyrins exhibited clearly in vitro cytotoxic activities against head and neck squamous cell carcinoma. Especially, free-base porphyrin-triazine hybrid **2** exhibited much smaller IC_{50} values by using CAL-27 (0.33±0.06 μg/mL) and CAL-33 (0.021±0.0007 μg/mL), respectively. In addition, their cell photoluminescence properties were also investigated.*

Keywords: Porphyrin-triazine hybrid, electronic structure, cytotoxic activities, fluorescent cell imagines.

Гибрид порфирин-триазин и его цинковый комплекс: спектроскопия, электрохимия и цитотоксическая активность *in vitro* против плоскоклеточного рака головы и шеи

Чжоуцюнь Цзи,[a] Интань Чжай,[b] Тинтин Гу,[b] Сюй Лян[b@]

[a]*Госпиталь при Университете Цзянсу, Чжэньцзян 212000, Китайская Народная Республика*
[b]*Школа химии и химического машиностроения, Университет Цзянсу, Чжэньцзян 212013, Китайская Народная Республика*
[@]*E-mail: liangxu@ujs.edu.cn*

*В данной работе были синтезированы и охарактеризованы гибрид порфирин-триазин **2** и его цинковый комплекс **2-Zn**, а также исследованы электронные структуры с помощью спектроскопических и электрохимических методов. Были подтверждены слабые взаимодействия между порфириновыми ядрами и мезозамещенными триазиновыми звеньями, а также обсуждено влияние растворителей на спектроскопические свойства. Важно отметить, что эти два порфирина продемонстрировали явную цитотоксическую активность in vitro против плоскоклеточного рака головы и шеи. В частности, гибрид порфирин-триазин **2** в форме свободного основания показал значительно меньшие значения IC_{50} при использовании CAL-27 (0,33±0,06 мкг/мл) и CAL-33 (0,021±0,0007 мкг/мл) соответственно. Кроме того, были исследованы их фотолюминесцентные свойства.*

Ключевые слова: Гибрид порфирин-триазин, электронная структура, цитотоксическая активность, флуоресцентные клеточные изображения.

Introduction

Porphyrins are a class of highly conjugated, aromatic macrocycles renowned for their structural robustness, rich photochemistry, and versatile coordination chemistry.[1,2] Found in nature as the active centers of chlorophyll and heme, synthetic porphyrins offer a nearly ideal "molecular canvas."[3] As an important branch of porphyrin, the porphyrins with special *meso*-substitutions exhibited versatile platforms for biochemical applications. Firstly, *meso*-substituted porphyrins have emerged as indispensable molecular platforms in modern biochemical research and biomedical applications. Unlike naturally occurring porphyrins which feature *β*-pyrrolic substitutions, synthetic porphyrins bearing functional groups at the four *meso*-positions (5,10,15,20) offer unparalleled synthetic accessibility, structural diversity, and tunable photophysical properties.[4-6] As established in foundational reviews, these compounds "present a readily accessible class of porphyrins which has found wide applications in biomedical sciences," with contemporary synthetic methodologies enabling "the generation of large libraries of compounds with variable *meso*-substituents or the preparation of bioconjugates".[7] In addition, the dominance of *meso*-substituted porphyrins in biochemical applications derives fundamentally from robust and versatile synthetic methodologies. Previously, researchers have highlighted that *meso*-formyl, vinyl, and ethynyl porphyrins serve as "multipotent synthons" for obtaining diverse functional derivatives through transformations of unsaturated carbon-oxygen and carbon-carbon bonds. The aldehyde group, in particular, is described as "rich in the possibilities of further transformations leading to the addition of functional fragments," enabling access to Schiff bases, Wittig products, and extended conjugated systems.[8] On the other hand, the *trans*-substituted 5,15-porphyrins, the Lindsey methodology – involving stoichiometric condensation between aldehydes and selected dipyrromethanes in the presence of acid catalysts followed by quinone oxidation – offers distinct advantages including ease of purification and potential for large-scale production.[9] More importantly, beyond direct photocytotoxicity, *meso*-substituted porphyrins exhibit sophisticated interactions with biological macromolecules that underpin both therapeutic efficacy and diagnostic applications. Copello and colleagues systematically evaluated *trans*-substituted 5,15-porphyrins using multi-spectroscopic techniques combined with molecular docking calculations.[7] Also, the synthetic versatility of *meso*-substituted porphyrins enables their integration into advanced drug delivery and theranostic platforms. Bortnevskaya and colleagues reported a sophisticated approach combining *meso*-arylporphyrins with the EGFR inhibitor Erlotinib via variable-length spacers, encapsulated within Pluronic F127 nanomicelles, and the confocal microscopy revealed that cationic pyridyl-containing derivatives showed pronounced colocalisation with early endosome antigen (EEA1), and the lead compound inhibited EGFR phosphorylation – demonstrating true dual-functionality as both photosensitiser and targeted therapeutic.[10] On the other hand, triazine, a versatile nitrogen-containing heterocycle, is of significant importance in biomedical applications due to its broad pharmacological potential. Triazine derivatives (1,2,4- and 1,3,5-isomers) demonstrate a wide spectrum of therapeutic activities, including anticancer, antimicrobial, antiviral, anti-HIV, antimalarial, anti-inflammatory, anti-tubercular, and anti-leishmanial properties. Several approved drugs contain the triazine core, including the anticancer agent altretamine, the anticonvulsant lamotrigine, the antimalarial cycloguanil, and the hypoxia-selective cytotoxin tirapazamine.[11-14] Interestingly, when triazine units were appended to the porphyrin cores, their novel molecular structures and useful synthetic methodologies have been attracted great attentions.[15-18] Also, their potential applications on the material and biomedical sciences were also highly interestingly for researchers in the related field.[19-20] Based on the above all advantages of porphyrins on the biomedical applications, especially the triazine appended porphyrin hybrids. We hereby provided an in-depth understand the electronic structure investigations by using a series of spectroscopic and electrochemical characterizations. Also, the *in vitro* cytotoxic activities against head and neck squamous cell carcinoma and fluorescent cell imagines were also discussed.

Experimental

General

High-resoution ESI-mass measurements were recorded on the LTQ-Orbitrap Elite machine. ^{1}H NMR and ^{13}C NMR spectra were recorded using a Bruker AVANCE 400 spectrometer operating at 400.03MHz (^{1}H NMR) and 100.06 MH_Z (^{13}C NMR), respectively. Chemical shifts (δ) were referenced to the residual solvent peaks as internal standards. All reagents and solvents were of reagent grade and used as received unless otherwise stated. UV-vis absorption spectra were measured using an HP 8453A diode array spectrophotometer. Electrochemical measurements were recorded on the CHI-730D electrochemical stations.

Synthesis

The general synthetic procedures are outlined in Scheme 1. The key precursor 5-(*p*-aminophenyl)-10,15,20-phenylporphyrin **1** was synthesized according to the literature reported procedure according to Scheme 1(a).[21]

*Porphyrin-Triazine hybrid **2**.* 5-Aminophenyl-10,15,20-phenylporphyrin **1** (50 mg, 0.08 mmol), 2,4,6-trichloro-1,3,5-triazine (30 mg, 0.16 mmol, 2.0 eq) and K_2CO_3 (75 mg, 0.55 mmol, 7.0 eq) were dissolved in 40 mL of $CHCl_3$, and the mixture was stirred at room temperature for 0.5 h. After quenching the reactions by water, the organic phase was washed with water (50 mL×3). After removal of organic solvent, the residue was purified by silica gel column chromatography (200–300 mesh; ethylacetate:hexane = 1:4, v:v) to give the pure porphyrin-triazine hybrid **2** as the solid state compound in a 74.7% yield (46.5 mg). ^{1}H NMR (400 MHz, $CDCl_3$) δ_H ppm: 8.91–8.81 (m, 8H), 8.58 (s, 1H), 8.26 (dd, *J* = 18.2, 10.0 Hz, 8H), 7.95 (d, *J* = 6.8 Hz, 2H), 7.82–7.72 (m, 9H), –2.77 (s, 2H). High-resolution ESI-mass *m/z*: 777.2042 (calcd. for $C_{47}H_{31}Cl_2N_8$ $[M+H^+]^+$ 777.1970). Elemental analysis: C, 72.88; H, 3.96; N, 14.31 (Calcd. for $C_{47}H_{31}Cl_2N_8$ C, 72.59; H, 3.89; N, 14.41).

*Porphyrin-Triazine hybrid zinc complex **2-Zn**.* Porphyrin-triazine hybrid **2** (28 mg, 0.036 mmol) and $ZnAc_2{\cdot}2H_2O$ (40 mg, 0.18 mmol) were dissolved in a mixed solution (CH_3OH:$CHCl_3$, 1:3, v:v), and the mixture was reacted at 30 °C under N_2. After removal of organic solvent, the residue was purified by silica gel column chromatography (200–300 mesh; ethylacetate:hexane = 1:4, v:v) to give the pure product as the purple solid state compound in a 76.3% yield (23.1 mg). ^{1}H NMR (400 MHz, $CDCl_3$) δ_H ppm: 8.96 (dd, *J* = 5.7, 4.2 Hz, 8H), 8.59 (s, 1H), 8.24 (dd, *J* = 17.0, 7.7

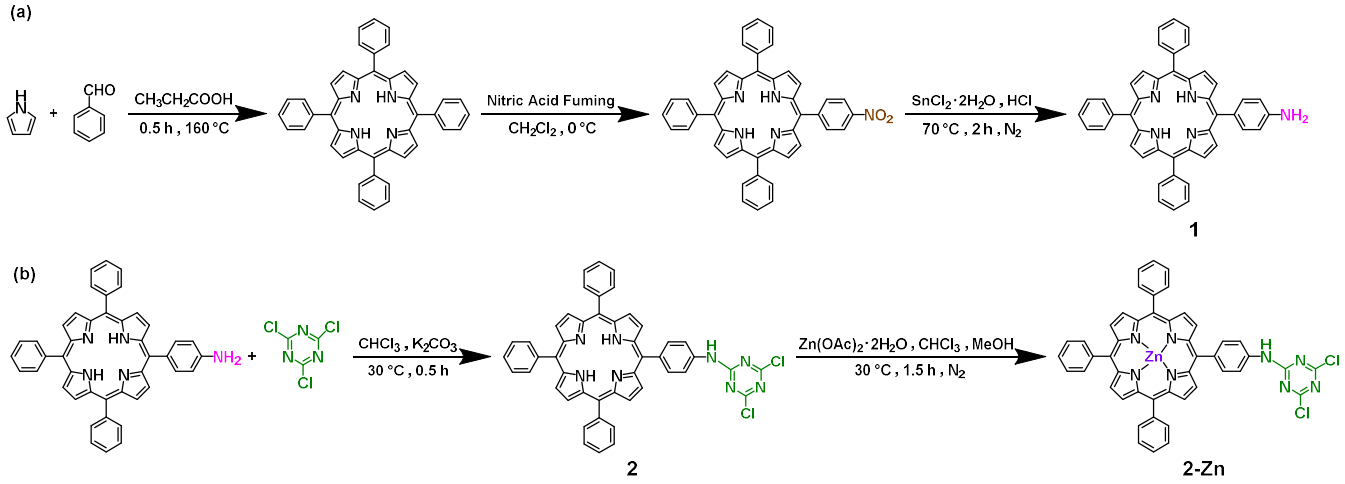

Scheme 1. The synthetic procedure of (a) 5-aminophenyl-10,15,20-phenylporphyrin **1**; (b) porphyrin-triazine hybrid **2** and its zinc complex **2-Zn**.

Hz, 8H), 7.96 (d, J = 4.3 Hz, 2H), 7.81–7.72 (m, 9H). High-resolution ESI-mass m/z: 839.1173 (calcd. for $C_{47}H_{29}Cl_2N_8Zn$ $[M+H^+]^+$ 839.1105). Elemental analysis: C, 67.25; H, 4.02; N, 14.17 (Calcd. for $C_{47}H_{28}Cl_2N_8$ Zn: C, 67.12; H, 3.36; Cl, 8.43; N, 13.32). ^{13}C NMR (100 MHz, $CDCl_3$) δ_C ppm: 172.590, 171.594, 171.210, 170.374, 167.751, 164.193, 150.335, 150.237, 150.061, 142.760, 140.346, 135.443, 135.144, 134.457, 132.210, 132.147, 132.113, 131.718, 130.936, 128.861, 127.569, 126.598, 121.401, 121.301, 119.736, 119.048, 65.603, 65.201, 60.425, 56.951, 56.071, 34.816, 34.530, 31.953, 31.539, 31.462, 30.594, 30.169, 30.130, 29.727, 29.390, 22.723, 21.036, 19.211, 14.210, 14.153, 13.759.

MTT measurements

Human CAL-27 and CAL-33 tumor cell lines were obtained from the Cell Bank of the Chinese Academy of Sciences (Shanghai, China) and BeNa Culture Collection (Beijing, China), respectively. The cells were cultured in DMEM medium supplemented with 10% fetal bovine serum and 100 U/mL penicillin under standard conditions (37 °C, 5% CO_2). For cytotoxicity assessments, cells were seeded in 96-well plates at 4×10^3 cells per well and treated with porphyrins **2** and **2-Zn** at specified concentrations. After a 24- or 48-hour incubation at 37 °C, 10 μL of MTT solution (5 mg/mL, 3-(4,5-dimethylthiazol-2-yl)-2,5-diphenyltetrazolium bromide) was added to each well. Following 1.5 hours of incubation, the unreacted dye supernatant was carefully removed, and 100 μL of DMSO was added to solubilize the formazan crystals. The optical density was measured at 590 nm with background correction at 630 nm using a microplate reader. Notably, each experiment was performed independently at least three times.

Fluorescent Cell Imagines

Human CAL-27 and CAL-33 cells in optimal growth condition (3×10^5 cells/well) were seeded into wells of a 24-well plate containing glass coverslips and incubated overnight in a humidified incubator (37 °C, 5% CO_2). The following day, the experimental group was treated with DMEM medium containing test compounds dissolved in DMSO to achieve a final concentration of 10 μM. In contrast, the control group received medium supplemented with an equivalent volume of DMSO. After 4 hours of incubation, the glass coverslips were carefully removed, washed, and fixed with 4% paraformaldehyde. The cells were stained with DAPI (4′,6-diamidino-2-phenylindole), and ProLong Diamond Antifade Mountant (PDD) was applied as an antifade mounting medium. The samples were examined under a fluorescence microscope after the mounting medium solidified.

Results and Discussion

Synthesis and Characterizations

Porphyrin-triazine hybrid **2** and its zinc complex **2-Zn** were obtained in the moderate yields around 76%, for which we have similar synthetic yield reported previously[11-18] and no multisubstituted derivatives were obtained under current conditions. To more-detailed confirm the molecular structure, high-resolution ESI-mass (Figures S1-S2, details see *Supporting Information*) of **2** and **2-Zn** revealed the strong patent peaks at m/z = 777.2042 (calcd. for $C_{47}H_{31}Cl_2N_8$ $[M+H^+]^+$ 777.1970) and m/z = 839.1173 (calcd. for $C_{47}H_{29}Cl_2N_8Zn$ $[M+H^+]^+$ 839.1105), respectively. The above clear mass data directly supported the target compounds were successfully prepared and isolated. The proton signals for the *meso*-substituents and pyrrole rings in the ^{1}H NMR spectra (Figures S3-S4, details see *Supporting Information*) of **2** and **2-Zn** mainly lie beyond 7.30 ppm, and the inner N-H proton signals were appeared at –2.80 ppm. Meanwhile, we also confirmed the ^{13}C NMR spectra of **2-Zn** (Figure S5) to assign all carbon signals from the target compounds. In addtion, the FT-IR spectra of **2-Zn** was also tested. As shown in Figure S6, the peak at around 800 cm^{-1} could be assigned as the C-Cl bond vibration absorption peaks, and halogenated arenes replacing *meta*-substituted positions exhibit a strong absorption between 1500–1600 cm^{-1}. Also, the purity was also confirmed by elemental analysis, and the consistency between theory and calculated values proves that the purity of the product meets the requirements.

Electronic Structure

As shown in Figure 1, the UV-visible absorption spectra of porphyrin-triazine hybrid **2** and its zinc complex were characterized. By comparing the spectroscopic properties of porphyrin **2** with the regular *meso*-tetraphenylporphyrin (Figure S7), the shape of the bands at λ = 648, 593, 550 and 515 nm at the Q band region, and λ = 420 nm at the B-band region are very similar to those of regular *meso*-tetraphenylporphyrin (Figure S7), and only a slight blue-shift of the absorptions was observed. This could be explained as the weak interactions between the triazine unit and porphyrin cores. Similarly, the zinc complex **2-Zn** also exhibited the slight blue-shift of the Q-band (λ=591 and 551 nm) and Soret-band absorptions (λ=425 nm) compared with the regular zinc tetraphenylporphyrin. In addition, we also tested the UV-vis absorption spectra of **2** and **2-Zn** in various solvents. As shown in Figure 2 and Table 1, when a series of four organic solvents with different polarities were applied, the similar shape and peak wavelength were obtained. Specially, when the PBS/10%DMSO was tested, the broader range of absorption bands and peak wavelengths were observed. More importantly, these two porphyrin were also emitted. As shown in Figure 1, Table 2 and Figure S8, porphyrin-triazine hybrid **2** (λ = 653 and 717 nm) and zinc complex **2-Zn** (λ = 600 and 647 nm) were exhibited mirror-imagine fluorescence bands behind the Q-band absorptions. Although the fluorescence properties reflect the structural dynamics in the excited state rather than the ground state, the observed properties are also similar to those of *meso*-tetraphenylporphyrin. This implies that there are weak interactions between the porphyrin ring and *meso*-substited triazine units.[12] Also, we confirm the fluorescent properties of **2** and **2-Zn** in various organic solvents, the shape of fluorescent peaks are quite similar in different solvents, but the red-shift of the emission peaks were observed in higher polar solvents. Also, the higher fluorescent quantum yield Φ_F and fluorescence life time τ_F (ns) were obtained in medium polar and aprotic solvents. Based on the above investigations, the weak interactions between porphyrin cores and triazine units were confirmed, and influence of solvents on the spectroscopic properties were also discussed.

In order to in-depth understand the electronic structure of porphyrin-triazine hybrid **2** and its zinc complex **2-Zn**, the electrochemical measurements were carried out in CH_2Cl_2 containing 0.1 M TBAP to gain further insight into the electronic properties, and the redox potential values were derived from both cyclic voltammetry and differential pulse voltammetry (CV and DPV) measurements.

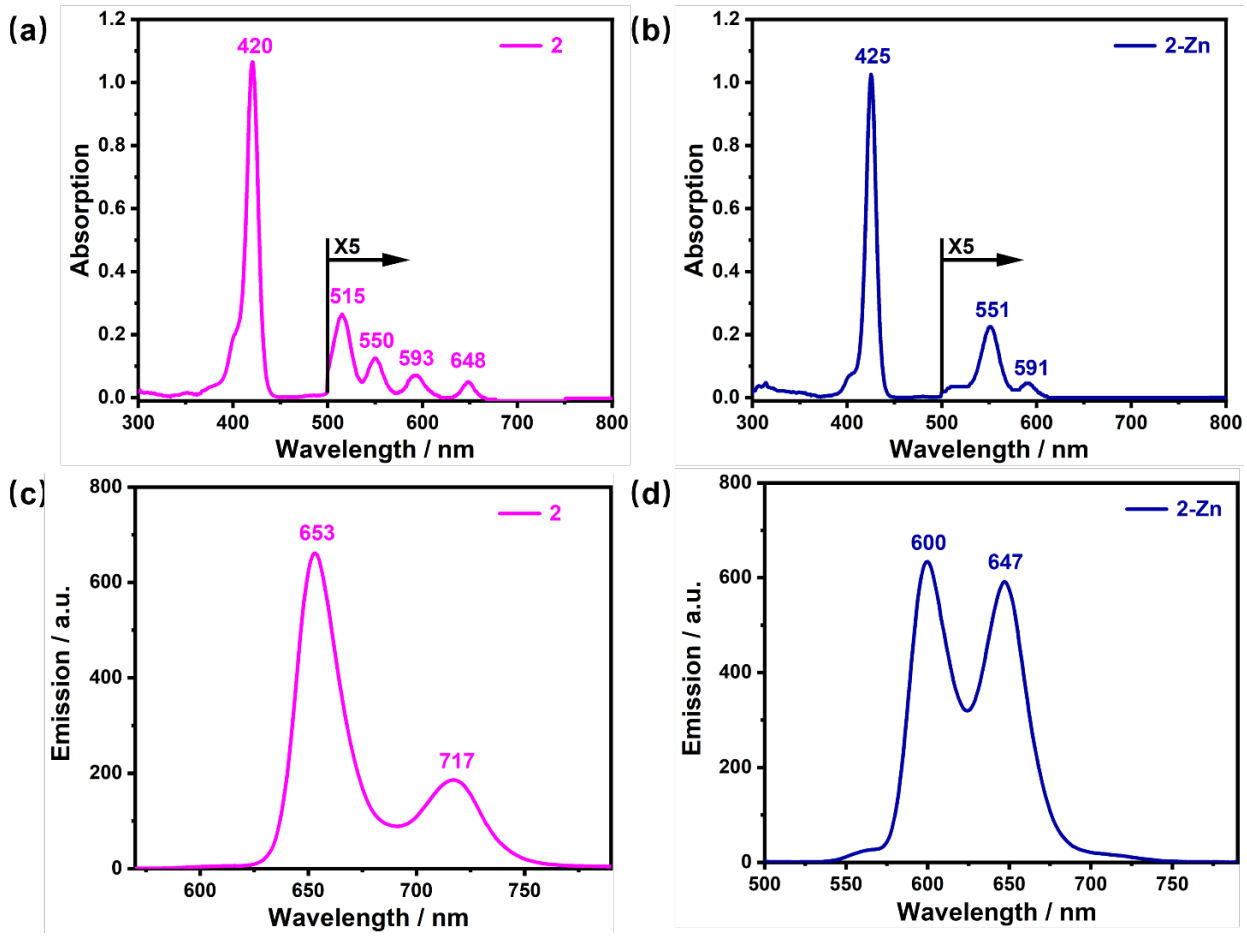

Figure 1. UV-vis absorption (up) and fluorescence (bottom) spectra of porphyrin-triazine hybrid **2** (a-b) and its zinc complex **2-Zn** (c-d) in toluene.

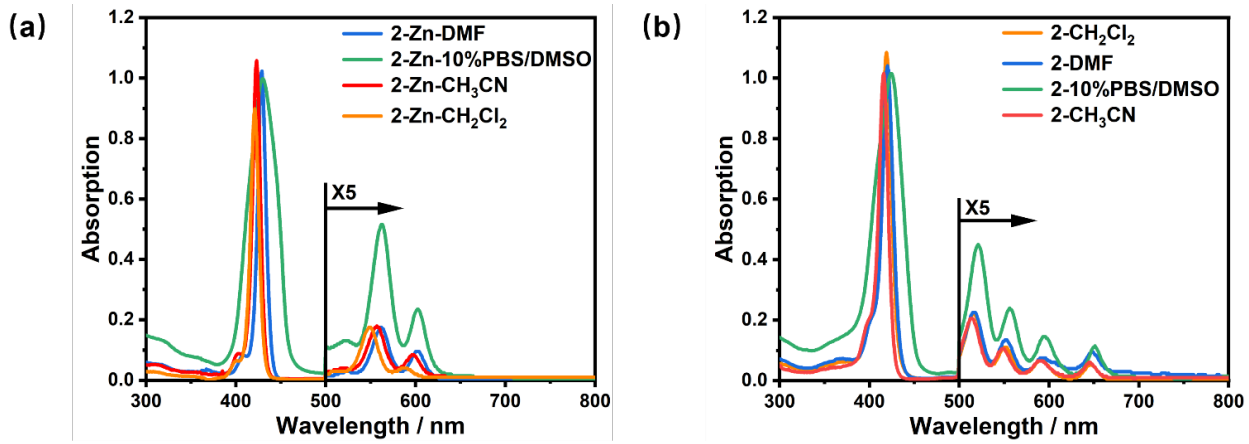

Figure 2. Normalized UV-vis absorption spectra of porphyrin-triazine hybrid **2** (a) and its zinc complex **2-Zn** (b) in various solvents.

Table 1. A summary of UV-vis absorption peaks wavelents of **2** and **2-Zn** in different solvents.

Compound	Solvent	Wavelength (nm)
2	CH_2Cl_2	419, 516, 552, 591, 647
2	Toluene	420, 515, 550, 593, 648
2	CH_3CN	416, 514, 549, 590, 645
2	DMF	420, 517, 552, 593, 648
2	PBS/10%DMSO	424, 521, 556, 595, 651
2-Zn	CH_2Cl_2	421, 549, 588
2-Zn	Toluene	425, 551, 591
2-Zn	CH_3CN	423, 557, 597
2-Zn	DMF	429, 561, 602
2-Zn	PBS/10%DMSO	430, 563, 603

Table 2 A summary of fluorescent properties of **2** and **2-Zn** in various solvents.

Solvent	λ_{em}, nm	Φ_F	τ_F, ns
PBS/10%DMSO	608, 660	0.0098*	0.82
Toluene	605, 658	0.0451*	2.06
CH_2Cl_2	597, 645	0.0214*	1.77
DMF	606, 658	0.0308*	2.11
CH_3CN	599, 648	0.0215*	1.80

As shown in Figure 3, the voltammogram for porphyrin-triazine hybrid **2** contains three reversible one-electron reduction steps at $E_{1/2}$ = –1.24, –1.77 and –1.89 V, respectively. Also, porphyrin **2** exhibited two reversible oxidation processes at $E_{1/2}$ = 0.84 and 1.12 V, respectively. On the other hand, the zinc complex **2-Zn** also revealed $E_{1/2}$= =–1.24, –1.73 and –1.87 V, and two oxidation processes at $E_{1/2}$ = 0.77 and 1.13 V. Comparing with previous reported regular *meso*-tetraphenylporphyrins and their zinc complexes, the redox potential values of **2** and **2-Zn** similar to those observed for monomeric complexes.[22] These results could be explained as the weak interactions between porphyrin cores and *meso*-substituted trazine units which are consistent with the results obtained from the spectroscopic investigations. In addition, i_p^{Red} and i_p^{Ox} values, determined from CV measurements for **2** and **2-Zn** made at various scan-rates from 50–500 mV (Figure S8, details see *Supporting Information*), provide an insight into the reversibility of the system on an experimental time-scale. The good linear correlations observed for plots of peak current *vs.* v½ for **2** and **2-Zn** (Figure S9) confirm that all of the oxidation and reduction processes are diffusion controlled.

MTT against CAL-27 and CAL-33 cells

CAL-27 and CAL-33 are both human tongue squamous cell carcinoma lines, widely used to study oral cancer. Although similar in origin and growth conditions, they have important genetic and functional differences that make them useful for different research questions. CAL-27 is known for being p53 wild-type and having high EGFR expression, making it a standard choice for studying EGFR-targeted therapies and general drug screening. It grows robustly and predictably in the lab. CAL-33, in contrast, carries a p53 mutation and is often described as more invasive and aggressive. It's particularly valuable for research on metastasis, drug resistance, and the consequences of p53 dysfunction. Thus, methylthiazolyldiphenyl-tetrazolium bromide (MTT) assays were performed to evaluate the anticancer activities of porphyrin-triazine hybrid **2** and its zinc complex **2-Zn** against CAL-27 and CAL-33 tumor cells in vitro. The in vitro cytotoxic activities of **2** and **2-Zn** against tumor cells were quantitatively compared using IC_{50} values, which are commonly used parameters for

evaluating the cytotoxic effectiveness of compounds. The IC_{50} value is defined as the drug concentration required to inhibit 50% of tumor cell proliferation in vitro, serving as a critical benchmark for comparing pharmacological efficacy. Before MTT investigations, the che-mical stability of **2** and **2-Zn** were tested by dissolving them in a PBS/DMSO mixed solvent (90:10, p*H* = 7.44) and incubating at 37°C for 24 hours in the absence of light. As shown in Figure S10, a similarity of over 96% proves that the product has ideal stabilities of **2** and **2-Zn** under current conditions.

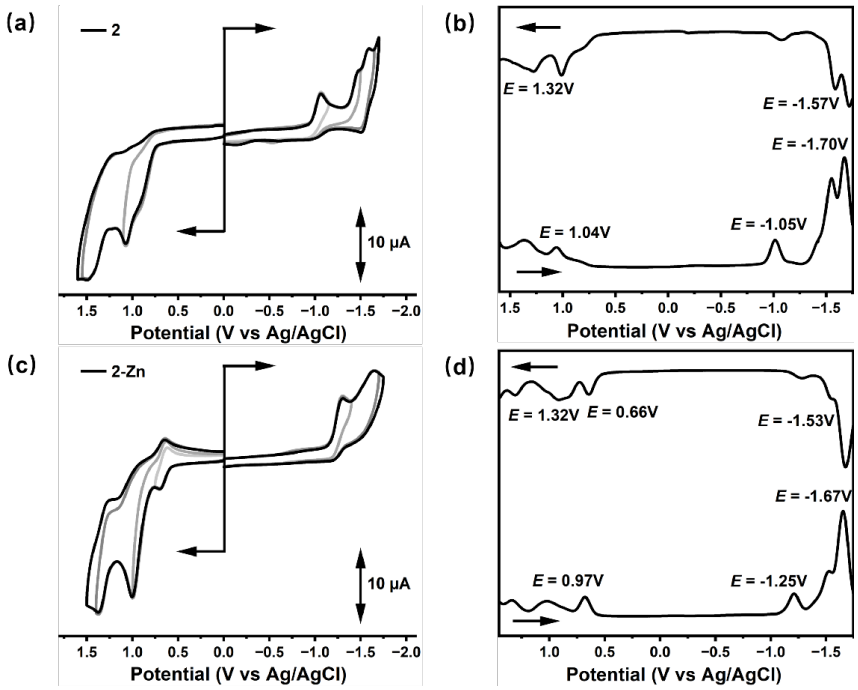

Figure 3. Cyclic voltammetry (up) and DPV (bottom) measurements of porphyrin-triazine hybrid **2** (a-b) and its zinc complex **2-Zn** (c-d) in CH_2Cl_2 containing 0.1M TBAP.

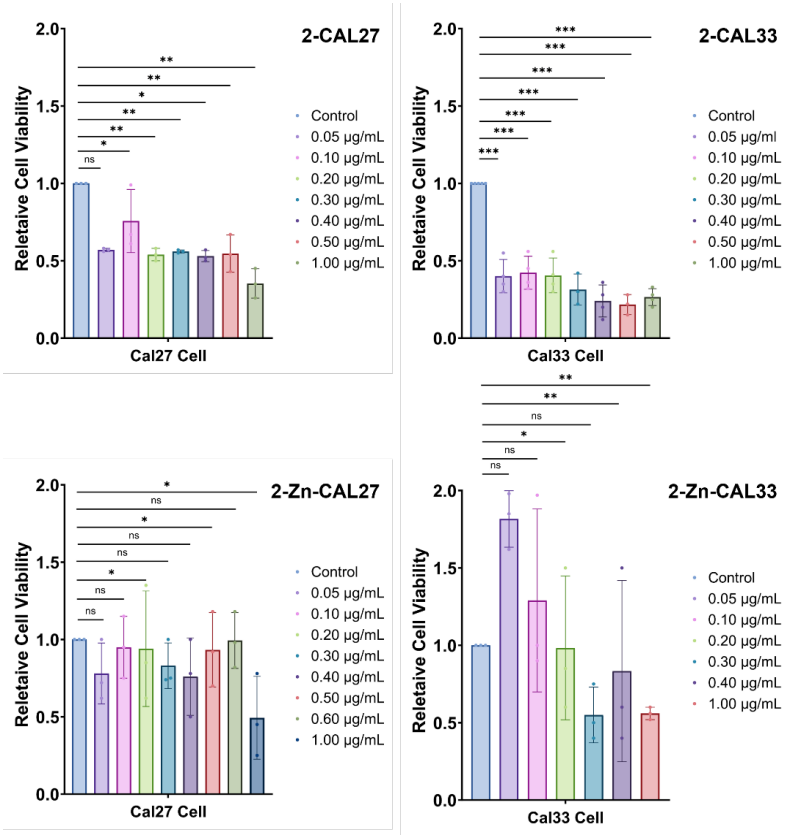

Figure 4. The inhibitory effect of porphyrin-triazine hybrid **2** and its zinc complex **2-Zn** on the in vitro proliferation of CAL-27 and CAL-33 tumor cells, with the detection time points being 24 hours, respectively.

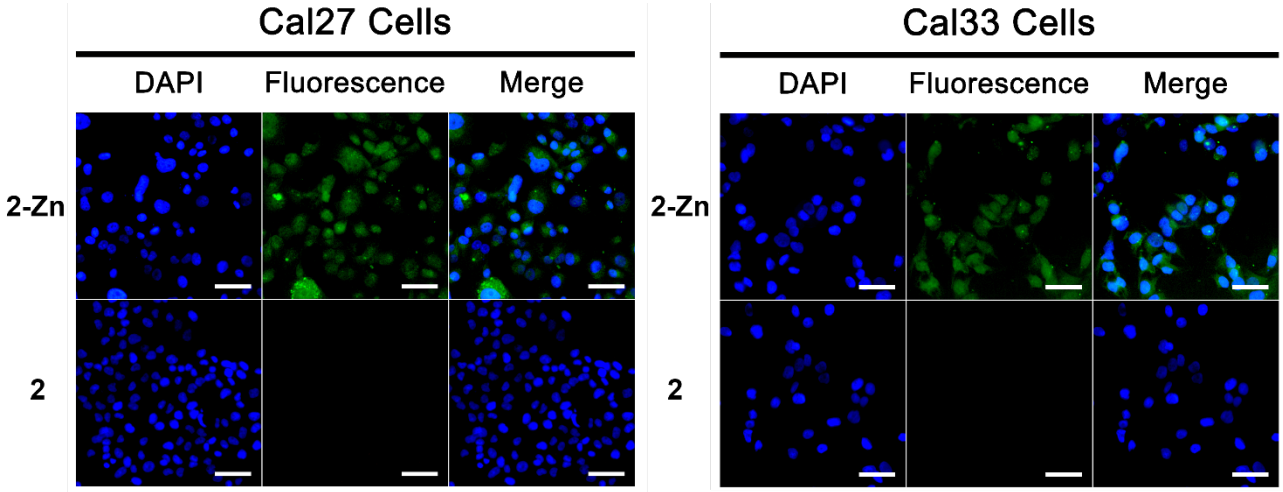

Figure 5. The fluorescent images of CAL-27 and CAL-33 tumor cells treated by DAPI, porphyrin-triazine hybrid **2** and its zinc complex **2-Zn** for 4h and the merged imagines.

As shown in Figure 4, porphyrin-triazine hybrid **2** and its zinc complex **2-Zn** exhibited potential cytotoxic activities against CAL-27 and CAL-33 tumor cells in the absence of light. When porphyrin-triazine hybrid **2** was used, the 4h IC_{50} values against CAL-27 and CAL-33 tumor cells are 0.33±0.06 μg/mL and 0.021±0.0007 μg/mL, respectively. Meanwhile, zinc porphyrin **2-Zn** exhibited its 4h IC_{50} values for 1.112±0.2 μg/mL (CAL-27) and 0.35±0.08 μg/mL (CAL-33), respectively. Importantly, porphyrin-triazine hybrid **2** has the better performance compared with that of **2-Zn**. The fundamental reason is that zinc coordination reduces the affinity of the molecule for mitochondria, leading to the transfer of toxic targets from the "lethal zone (mitochondria)" to the "relatively tolerant zone".[23-24]

In addition, the fluorescent cell imagines were also investigated to validate the interaction between porphyrin-triazine hybrid **2**, zinc complex **2-Zn** and CAL-27/CAL-33 tumor cells. After 4 h of chemical treatment of **2**/**2-Zn** and CAL-27/CAL-33 tumor cells, the active cells were fixed with 4% formaldehyde for 10 min and washed with PBS solutions. Then, CAL-27/CAL-33 cells were stained with 1 μg/μL DAPI (4′,6-diamidino-2-phenylindole, Mannheim, Baden-Württemberg, Germany), and all immunofluorescent photo images were collected from a Nikon Eclipse (Minato-ku, Tokyo, Japan) microscope. As shown in Figure 5, DAPI exhibits complete cell membrane permeability, enabling dual staining applications in both live and fixed-cell systems. Strikingly, pronounced luminescent signals were exclusively detected in sample images and multichannel overlays from green channel detectors when zinc porphyrin **2-Zn** was administered. This could be assigned the S_2-S_0 emission of **2-Zn** in the living cells. Considering porphyrins **2** and **2-Zn** have the robust chemical stability and bio-capabilities, the unprecedented fluorescent cell imagines could be explained as the fluorescence quenching of porphyrin **2**.

Conclusion

In summary, a porphyrin-triazine hybrid **2** and its zinc complex **2-Zn** were prepared and their structural information was confirmed by high-resolution ESI-mass, ^{1}H and ^{13}C NMR spectra, FT-IR spectra and elemental analysis. In addition, the electronic structures of **2** and **2-Zn** were indetailed characterized by a series of spectroscopic and electrochemical methods. Importantly, the weak electronic interactions between porphyrin core and *meso*-substituted triazine units were confirmed, and the influence of solvents on the spectroscopic properties was also revealed. More interestingly, these two porphyrins exhibited clearly *in vitro* cytotoxic activities against head and neck squamous cell carcinoma, the 4 h IC_{50} values of against CAL-27 and CAL-33 tumor cells are 0.33±0.06 μg/mL and 0.021±0.0007 μg/mL, which are better than zinc porphyrin **2-Zn** exhibited its 4 h IC_{50} values for 1.112±0.2 μg/mL and 0.35±0.08 μg/mL. This may be due to zinc coordination reduces the affinity of the molecule for mitochondria, leading to the transfer of toxic targets from the "lethal zone (mitochondria)" to the "relatively tolerant zone". Meanwhile, the fluorescent imagines were also tested. Considering the porphyrins can be widely applied in various fields, the current research may provide useful information for future investigations on the relationship between molecular structure and electronic structure, and their potential applications of *in vitro* cytotoxic activities and fluorescent imagines.

Author contributions. Zhouqun Ji and Yingtan Zhai are contributed to the spectroscopic and biomedical investigations, and Tingting Gu was focused on the compound preparation. Xu Liang supervised the project. All authors prepared, discussed, and approved the whole manuscript.

Acknowledgements. This work was supported financially by the National Natural Science Foundation of China (21701058) and the Innovation Project of Jiangsu Province 2023. Theoretical calculations were carried out at Jiangsu University using laboratory computers.

Conflicts of interest. The authors declare that no known competing personal relationships or financial interests could be perceived to have influenced the research reported in this study.

References

1. Chizhova N.V., Likhonina A.E., Tesakova, M.V., et al. *J. Mol. Struct.* **2025**, *1335*, 141998.
2. Majumder S., Borah B.P., Bhuyan J. *Dalton Trans.* **2020**, *49*, 8419–8432.
3. Chen H., Wang Y., Wang W., et al. *Nat. Biotechnol.* **2025**, *43*, 1717–1727.
4. Hiroto S., Miyake Y., Shinokubo Y. *Chem. Rev.* **2017**, *117*, 2910–3043.
5. Lu H., Kobayashi N. *Chem. Rev.* **2016**, *116*, 6184–6261.
6. Han J.L., Liu Y.D., Peng D.F., et al. *Bioconjugate Chem.* **2023**, *34*, 2155–2180.
7. Bortnevskaya Y.S., Zakharov N.S., Senkov V.S., et al. *Mol. Pharm.* **2025**, *22*, 3308–3330.
8. Tyurin V.S,, Shkirdova A.O., Koifman O.I., et al. *Molecules* **2023**, *28*, 5782.
9. Brém B., Gal E., Găină L., et al. *RSC Med. Chem.* **2024**, *16*, 747–766.
10. Balukova A., Bokea K., Barber P. R., et al. *Int. J. Mol. Sci.* **2024**, *25*(8), 4222.
11. Dubey P., Pathak D. P., Ali F., Chauhan G., Kalaiselvan V. *Curr. Drug Discov. Technol.* **2024**, *21*, e170723218813.
12. Kumawat J., Jain S., Misra N., et al. *Mini Rev. Med. Chem.* **2024**, *24*, 2019–2071.
13. Rathod B., Pawar S., Puri S., et al. *ChemistrySelect* **2024**, *9*, e202303655.
14. Tountas M., Verykios A., Polydorou E., el al. *ACS Appl. Mater. Interfaces* **2018**, *10*, 20728–20739.
15. Alpatova V.M., Rys E.G., Kononova E.G., et al. *Molecules* **2022**, *27*, 6200.
16. Lazarides T., Charalambidis G., Vuillamy A., et al. *Inorg. Chem.* **2011**, *50*, 8926–8936.
17. Xiao X.C., Liu C.Z., Liu W.K. et al. *J. Porphyrins Phthalocyanines* **2010**, *14*, 123–127.
18. Regmi N., Sharma M., Kumar S., et al. *J. Mol. Struct*. **2026**, *1350*, 14386
19. Manathanath M., Sasidharan S., Saudagar P., et al. *Polyhedron* **2022**, *217*, 115711.
20. Ringot C., Saad N., Granet R., et al. *Carbohydr. Polym*. **2013**, *91*, 333–338.
21. Liang X., Xu L., Li M.Z., et al. *J. Porphyrins Phthalocyanines* **2015**, *19*, 819–829.
22. Kadish K.M., Van Caemelbecke E., Royal G. In: *The Porphyrin Handbook*, *Vol. 8* (Kadish K.M., Smith K.M., Guilard R., Eds.), New York: Academic Press, **2000**. pp. 1–114.
23. Pavani C., Iamamoto Ya., Baptista M.S. *Photochem. Photobiol.* **2012**, *88*(4), 774–781.
24. Deda D.K., Pavani Ch., Caritá E., et al. *J. Porphyrins Phthalocyanines* **2012**, *16*(1), 55–63.

Received 17.01.2026
Accepted 09.03.2026